JOURNAL OF COMPUTATIONAL PHYSICS 47, 229–244 (1982)

Electron Sub-Cycling in Particle Simulation of Plasma

J. C. ADAM AND A. GOURDIN SERVENIERE

Centre de Physique Théorique de l'École Polytechnique, 91128 Palaiseau, France

AND

A. B. LANGDON

Lawrence Livermore National Laboratory, University of California, Livermore, California 94550

Received December 16, 1981

A straightforward modification which reduces by half the computational cost of standard particle-in-cell algorithms for simulation of plasmas is described. The saving is obtained by integrating only the electrons through a number of time steps (sub-cycles) in order to resolve their evolution, while integrating the much slower ions only once per cycle, i.e., to match the time step of each species to their characteristic frequencies. A dispersion relation is derived which describes the numerical instabilities expected by sampling frequency arguments. Simulations support the broad features of the analytical results, viz., the maximum growth rate and domain of the instability, and its stabilization by the addition of weak damping. An implicit sub-cycling algorithm is suggested which may provide further saving while avoiding a limitation of implicit algorithms described elsewhere.

1. INTRODUCTION

There is increasing interest in simulation of plasma phenomena developing on time scales that are very slow compared to the electron plasma oscillation frequency. The prevalent particle-in-cell simulation algorithms require a very large number of time steps in such applications, often making them an expensive tool. Our purpose here is to show that one can exploit the difference in inertia of ions and electrons to devise an easy modification to standard PIC codes that allows a gain of almost a factor of two in the computing time of any electrostatic model. In an electromagnetic model, where the relative cost of the ions is less important, the gain is somewhat smaller but is as easily obtained.

Unlike the implicit particle code algorithms [1, 2], which are intended to meet the same need, there is no limitation to wavelengths much larger than the Debye length, or to small field gradients, nor are high frequency electron waves eliminated. In fact, there exists a whole class of phenomena such as modelling of ion acoustic turbulence which requires the dynamics of both electrons and ions to be followed accurately.

The basis of the algorithm is to use a standard leapfrog scheme for pushing both

0021-9991/82/080229–16$02.00/0

electrons and ions, but the electron time step is a fraction of the ion time step. For each complete cycle of time integration, there is one cycle for the ions and several sub-cycles for the electrons. As the mass of ions makes them insensitive to high frequencies, one can use a larger time step for ions than electrons, which quickly makes the cost of pushing ions very low. We show, however, that frequency aliasing introduces numerical instabilities in some intervals of time step. The main purpose of this paper is to study these instabilities theoretically and numerically in order to determine the range of applicability of this algorithm and future schemes employing electron sub-cycling. We examine means to stabilize the algorithm. Examples of applications will be described elsewhere [3].

2. The Algorithm

As mentioned in the introduction, the basis of the algorithm is the fact that ions do not respond to the high frequency waves. This allows suppression of the high frequencies in the field seen by the ions and permits us to push them with a time-step larger than that used for electrons. We shall show that this can be done in a way that preserves centering in time. The ion time step Δt_i will be an integer multiple N of the electron time step Δt_e. When N is odd or even, we find slightly different schemes. In the most natural one, N is odd.

2.1 *Odd N Scheme*

The scheme is illustrated in Fig. 1a. For clarity we assume that $N = 3$ and that the ion density is defined at integer time in terms of ion time steps ($\rho_{i,0}, \rho_{i,1}, \ldots$, in Fig. 1a). The electron density is defined at integer time steps simultaneously with the ions, and at fractional time steps ($\rho_{e,1/3}, \rho_{e,2/3}, \ldots$ in Fig. 1a). More generally, the ion density is known at time $t_n = n\Delta t_i$ while the electron density is known at time $t_{n/N} =$

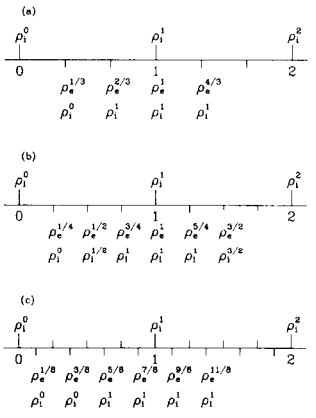

FIG. 1. Odd and even versions of the proposed sub-cycling algorithm. (a) odd N scheme; (b) even N scheme; and (c) even N scheme.

$(n/N)\,\Delta t_i = n\Delta t_e$ $(n = 0, 1, 2,...)$. Electrons are pushed from time $n\Delta t_i - M\Delta t_e$ to time $n\Delta t_i + M\Delta t_e$, where $M = (N-1)/2$, assuming ion positions as defined at time $n\Delta t_i$. The electric field seen by the ions is then computed as a function of the electric field calculated from the intermediate positions of electrons. Ions are then advanced one time step and the cycle is repeated. Recalling that, for the leapfrog scheme, positions and velocities are defined with a lag of half a time step, it is easy to see that this scheme is centered.

2.2 *Even N Scheme*

The most direct extension to even N of the odd N case just described is illustrated in Fig. 1b. Two inconvenient features appear immediately, however, on tracing through a complete cycle, which proceeds as follows: We begin with the electron positions known at time $t_{1/2}$ and the ions at time t_1. The first electron sub-cycle is based on the electric field at time $t_{1/2}$. To retain centering, this field presumably uses an average of $\rho_{i,1}$ and $\rho_{i,0}$ which must be retained from earlier. The remaining electron subcycles proceed simply to time $t_{3/2}$ using $\rho_{i,1}$. To obtain an electric field at time t_1 for integration of the ions, we use an approximation to the time average of ρ from $t_{1/2}$ to $t_{3/2}$. In these time averages, the electron densities $\rho_{e,1/2}$, $\rho_{e,3/2}$, etc. appear twice, used on successive cycles. This implies that a weight of $\frac{1}{2}$ should be used on the electric field at times $n - \frac{1}{2}$ and $n + \frac{1}{2}$ when computing the electric field seen by the ions. In fact, this is also what one would have using the trapezoidal integration formula to compute the electric field seen by the ions by summing the field defined by the successive positions of electrons over an ion time step.

Figure 1c presents an alternative to the preceeding even N scheme. It avoids the two inconveniences mentioned, but at the expense of a time lag of half an electron time step, which means that ions and electrons are never known at the same time. This may be a problem for diagnostics purposes. Otherwise it can readily be seen that it is strictly equivalent to the odd N scheme.

As we have found no advantages to offset the inconveniences found for even N, we shall use only odd values. A similar algorithm was considered by Dawson and co-workers [4].

2.3 *Filter Choices*

The electric field seen by the ions is defined as a function of the electric field seen by the electrons. The most obvious function is a time average of this field. In principle, however, more sophisticated filters can be chosen. One has to be careful to use only finite impulse response filters (i.e., nonrecursive) in order to maintain time centering. In fact, with the number of data points available for filtering during one ion time step, we find that it is difficult to do much better than averaging unless the mass ratio is very large. Moreover, in the next section we shall see that the introduction of an arbitrary filter in the algorithm instead of a simplex average can induce a strong instability in the vicinity of $\omega_{pe}\Delta t_i = 2\pi$.

3. Theoretical Analysis

In this section we derive a dispersion relation which predicts instabilities when $\omega_{pe}\Delta t_i$ is near π, 2π, and other multiples. Approximate analytical solutions are found which adequately estimate the maximum growth rates. In the next section, numerical solutions of the dispersion relation are presented which describe the instabilities more completely and accurately for comparison with results of actual simulations. We need not include the effects of the spatial grid as we do not anticipate interactions between spatial and temporal discretization in these problems; such a generalization is straightforward with existing methods [5].

3.1 *Derivation of the Dispersion Relation*

We assume $N = 2M + 1$ is odd, and label ion time steps by n, and electron time steps by n'. As the electrons are integrated from step $nN - M$ to $nN + M$, the electric field used is obtained from a charge density $\rho_{i,n} + \rho_{e,n'}$, i.e., the ion density at their nearest time $n\Delta t_i$, plus the electron density at the current electron step n'. Then the ions are integrated using the field calculated from $\rho_{i,n}$ plus a filtered electron density

$$\rho_{i,n} + \sum_{n'=-M}^{M} a_{n'}\rho_{e,n'+nN}, \tag{1}$$

where the filter coefficients are normalized, $\sum a_{n'} = 1$, and (normally) are symmetric, $a_{-n'} = a_{n'}$.

In order to derive the dispersion relation, we must relate Fourier transforms of ρ_i as perceived by the electrons, and the filtered ρ_e as perceived by the ions. Our transform conventions are, for the ions

$$\rho_i(\omega) = \Delta t_i \sum_n \rho_{i,n} e^{i\omega t_n}, \tag{2a}$$

$$\rho_{i,n} = \int_{-\pi/\Delta t_i}^{\pi/\Delta t_i} \frac{d\omega}{2\pi} \rho_i(\omega)\, e^{-i\omega t_n}, \tag{2b}$$

where $t_n = n\Delta t_i$, and similarly for the electrons. From (2a) we find the periodicities $\rho_i(\omega + 2\pi/\Delta t_i) = \rho_i(\omega)$ and $\rho_e(\omega + 2\pi/\Delta t_e) = \rho_e(\omega)$. We Fourier transform all fields in space and suppress the argument k.

The electric field used to integrate the electrons is given by the transformed Gauss' law with source $\rho_{e,n'} + \rho_{i,n}$, where n is the integer closest to n'/N. Transforming in time,

$$\begin{aligned} ikE_e(\omega) - \rho_e(\omega) &= \Delta t_e \sum_{n'} \rho_{i,n} e^{i\omega n'\Delta t_e} \\ &= \Delta t_e \sum_n \rho_{i,n} \sum_{n'=-M}^{+M} e^{i\omega(n'+nN)\Delta t_e} \\ &= \Delta t_i \sum_n \rho_{i,n} H_1(\omega)\, e^{i\omega t_n}, \end{aligned}$$

where

$$H_1(\omega) = \frac{1}{N} \sum_{n'=-M}^{M} e^{i\omega n' \Delta t_e} = \frac{\sin(\omega \Delta t_i/2)}{N \sin(\omega \Delta t_e/2)} \tag{3}$$

can be removed from the sum, leaving $\rho_i(\omega)$. Thus

$$ikE_e(\omega) - \rho_e(\omega) = H_1(\omega)\, \rho_i(\omega). \tag{4}$$

$H_1(\omega)$ has periodicity $2\pi/\Delta t_e$. Over such an interval, $\rho_i(\omega)$ repeats N times. Thus even if $\rho_{i,n}$ varies only with low frequencies $\ll \pi/\Delta t_i$, the electrons perceive the low frequencies, plus harmonics of $2\pi/\Delta t_i$. This is because ρ_i as seen by the electrons is piecewise constant with a jump every N steps.

The electric field used to integrate the ions is given by the transformed Gauss' law with source Eq. (1)

$$\begin{aligned} ikE_{i,n} - \rho_{i,n} &= \sum_{n'=-M}^{M} a_{n'} \rho_{e,n'+nN} \\ &= \sum_{n'} a_{n'} \int_{-\pi/\Delta t_e}^{\pi/\Delta t_e} \frac{d\omega}{2\pi} \rho_e(\omega)\, e^{-i\omega(n\Delta t_i + n'\Delta t_e)} \\ &= \int_{-\pi/\Delta t_e}^{+\pi/\Delta t_e} \frac{d\omega}{2\pi} \rho_e(\omega)\, H_2(\omega)\, e^{-i\omega t_n}, \end{aligned} \tag{5}$$

in which we have used the analog of (2b) for the electrons, and introduced the transfer function $H_2(\omega)$ for the filter $\{a_{n'}\}$,

$$H_2(\omega) = \sum_{n'=-M}^{M} a_{n'} e^{-i\omega n' \Delta t_e}. \tag{6}$$

We break the interval of integration in (5) into N subintervals of length $2\pi/\Delta t_i$

$$\begin{aligned} ikE_{i,n} - \rho_{i,n} &= \int_{-\pi/\Delta t_i}^{\pi/\Delta t_i} \frac{d\omega}{2\pi} \sum_{q=-M}^{+M} e^{-i\omega_q t_n} \rho_e(\omega_q)\, H_2(\omega_q) \\ &= \int \frac{d\omega}{2\pi} e^{-i\omega t_n} \sum_q \rho_e(\omega_q)\, H_2(\omega_q), \end{aligned} \tag{7}$$

where $\omega_q \equiv \omega - 2\pi q/\Delta t_i$; and we have used the periodicity of the factor $\exp(-i\omega_q t_n) = \exp(-i\omega t_n)$ to remove it outside the sum. Comparing (7) to (2b), we recognize

$$ikE_i(\omega) - \rho_i(\omega) = \sum_{q=-M}^{+M} \rho_e(\omega_q)\, H_2(\omega_q). \tag{8}$$

The linear charge density response to the electric field can be written in general as

$$\rho_i(\omega) = -ik\chi_i(\omega)\, E_i(\omega), \tag{9}$$

and similarly for the electrons. Evaluation of the susceptibility χ, including the effect of finite Δt, is given elsewhere [6]; the expressions we use are given in the next section. From (4) and (8),

$$-(1+\chi_e^{-1}(\omega))\,\rho_e(\omega) = H_1(\omega)\,\rho_i(\omega) \tag{10}$$

$$-(1+\chi_i^{-1}(\omega))\,\rho_i(\omega) = \sum_q \rho_e(\omega_q)\, H_2(\omega_q). \tag{11}$$

We use (10), with ω replaced by ω_q, to express ρ_e in (11). Then we use the periodicity of ρ_i to remove it from the sum. Cancelling ρ_i yields the dispersion relation

$$1+\chi_i^{-1}(k,\omega) = \sum_{q=-M}^{+M} \frac{H_1(\omega_q)\, H_2(\omega_q)}{1+\chi_e^{-1}(k,\omega_q)}. \tag{12}$$

As a check, we note that, for $N=1$, $H_1 H_2 = 1$ and we have $(1+\chi_i^{-1}) = (1+\chi_e^{-1})^{-1}$, or $1+\chi_e+\chi_i = 0$, the correct result. Also the coupling between electron modes implies by the sum ($N>1$) is entirely due to the ions, for when the ion plasma frequency $\omega_{pi} \to 0$, the left-hand side of (12) becomes infinite. The solutions of (12) are then simply the zeroes of each denominator $1+\chi_e^{-1}(k,\omega_q)$, i.e., of the dispersion relation for electrons only, replicated N times. We shall discuss the meaning of this multiplicity of roots, and then present numerical and approximate analytic solutions for the unstable cases $\omega_{pe}\Delta t_i \simeq \pi$ and 2π.

4. Solutions of Warm Plasma Dispersion Relation

We now find approximate roots analytically and accurate numerical solutions of (10) and (11) for later comparison with simulations. We assume cold ions, for which

$$\chi_i = \frac{(\omega_{pi}\Delta t_i)^2}{(2\sin(\omega\Delta t_i/2))^2}, \tag{13}$$

and warm electrons, for which [6]

$$\chi_e(k,\omega) = \frac{\omega_{pe}^2}{k^2}\int dvk\,\frac{\partial f_0}{\partial v}\,\frac{\Delta t_e}{2}\cot(\omega - kv)\,\frac{\Delta t_e}{2}. \tag{14}$$

In fact, we mostly used the approximation of χ_e which retains only second-order finite time step correction given in [6], i.e.,

$$\chi_e = \chi_0 - \tfrac{1}{12}(\omega_{pe}\Delta t_e)^2, \tag{15}$$

where χ_0 is the continuous result which can be expressed in terms of the Z' derivative of the Fried–Conte function in the case considered here of a plasma in thermodynamic equilibrium. We checked that in most cases the difference between this second-order expression and the exact solution was negligible. Effects due to a finite spatial grid are neglected. The results presented below are obtained in the case $a_n = 1/N$, for which $H_1 = H_2$.

4.1 *Interpretation of the Roots of the Dispersion Relation*

The solution ω is the frequence as the ions see it, with their larger time step. Electron frequencies $\omega \pm 2\pi/\Delta t_i$, $\omega \pm 4\pi/\Delta t_i$,..., all appear the same as ω to the ions, and all are roots of the dispersion relation if ω is a root. This is manifest in the periodicity properties of $\chi_{e,i}$ in Eqs. (13) and (14).

To see which frequencies are important to each species, consider $\chi_e(\omega - 2\pi q/\Delta t_i)$ terms contributing significantly to the dispersion relation in each particular case.

With $\omega_{pe}\Delta t_i \sim \pi$, consider first the root ω near $\pi/\Delta t_i$, then $e^{-i\omega t_n} \simeq e^{-in\pi} = (-1)^n$. Thus the ions feel an alternating *odd–even* dependence on time step. The electron terms that matter are those with $\chi_e(\omega)$ and $\chi_e(\omega - 2\pi/\Delta t_i)$, which are near $+\omega_{pe}$ and $-\omega_{pe}$. Thus the electrons contribution is two oppositely directed Langmuir waves.

What happens in this same case if one chooses instead the root ω of the dispersion relation near $5\pi/\Delta t_i$? For the ions, the time dependence is $e^{-i\omega t_n} \simeq \exp(-i[5\pi/\Delta t_i]\, n\Delta t_i) = (-1)^n$, the same as before. In the dispersion relation, the important electron terms are now q equals 2 and 3, so the frequencies ω_q in the relevant χ_e terms are $\omega_2 \simeq \pi/\Delta t_i \simeq \omega_{pe}$ and $\omega_3 \simeq -\pi/\Delta t_i \simeq -\omega_{pe}$, also as before. Therefore, this root corresponds to the same mode of this time-sampled system.

With $\omega_{pe}\Delta t_i \simeq 2\pi$, take for convenience the root ω near zero, so that the ions experience slowly varying fields. The important electron terms in the dispersion relation are those with $\chi_e(\omega)$, $\chi_e(\omega_1)$, and $\chi_e(\omega_{-1})$, i.e., electrons are responding to three frequencies: $\omega \ll \omega_{pe}$ and $\omega_{\pm 1} = \omega \pm 2\pi/\Delta t_i \simeq \pm\omega_{pe}$. Thus the electrons contribute in their usual way to the ion acoustic perturbation, which is coupled by the numerical method to two oppositely directed Langmuir waves.

4.2 *Study of Dispersion Relation Around* $\omega_{pe}\Delta t_i = \pi$

To find the maximum growth rate, we assume cold electrons and adjust $\omega_{pe}\Delta t_i$. Let ω be near $\omega_{pe} = \pi/\Delta t_i$, and define

$$\Omega = \omega - \pi/\Delta t_i$$

which is much smaller than Δt_e^{-1}. Then $\omega_1 = \Omega - \pi/\Delta t_i$. For these two frequencies,

$$\chi_e^{-1}(\Omega \pm \pi/\Delta t_i) = -[\sin(\pi/2N)(2/\omega_{pe}\Delta t_e)]^2 \mp (\Omega/\omega_{pe})\cos(\pi/2N),$$
$$H_1(\Omega \pm (\pi/\Delta t_i)) = (1/N\sin(\pi/2N)) + O(\Omega\Delta t_e); \tag{16}$$

and

$$\chi_i^{-1}(\Omega \pm (\pi/\Delta t_i)) = (2/\omega_{pi}\Delta t_i)^2 + O(1) \tag{17}$$

is much larger than one. Keeping only dominant terms, the dispersion relation becomes

$$-(2/\omega_{pi}\Delta t_i)^2 = 2H_1^2 A/(A^2 - 4\Omega^2/\omega_{pe}^2), \tag{18}$$

where

$$A = 1 - [(2/\omega_{pe}\Delta t_e)\sin(\pi/2N)]^2.$$

The maximum growth rate is given by

$$\mathrm{Im}(\omega/\omega_{pe}) = (\omega_{pi}/\omega_{pe})^2/2 \tag{19}$$

and it occurs when $A = -\omega_{pi}^2/\omega_{pe}^2$. Rewriting this and remembering that ω_{pe} in A should more accurately be the Bohm–Gross frequency, we have

$$(\omega_{pe}^2 + 3k^2V_e^2)(\Delta t_i^2/\pi^2) = ((2N/\pi)\sin\pi/2N)^2/(1 + \omega_{pi}^2/\omega_{pe}^2), \tag{20}$$

where the right-hand side is slightly less than unity. In summary, the largest growth rate is found for $\omega_{pe}\Delta t_i$ slightly less than π, and is smaller than ω_{pe} by the factor m_e/m_i.

In Figs. 2a and 2b, the growth rate of the instability is shown as a function of $\omega_{pe}\Delta t_i$ for two values of $k\lambda_D$ and a mass ratio $m_i/m_e = 100$. The value of $k\lambda_D = 0.015$ was chosen because, for such a small value, the cold plasma analysis should apply while the value $k\lambda_D = 0.0982$ corresponds to the simulations discussed in Section 5.

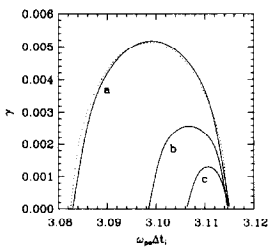

FIG. 2. (a) Growth rate of the numerical instability for $\omega_{pe}\Delta t_i$ in the vicinity of π as a function of the mass ratio for $k\lambda_D = 0.015$ and $\Delta t_i/\Delta t_e = 7$. The approximate analytical solution (···), and the numerical solution (—) of the exact dispersion relation; (a) is for a mass ratio $m_i/m_e = 100$, (b) for $m_i/m_e = 200$, and (c) for $m_i/m_e = 400$.

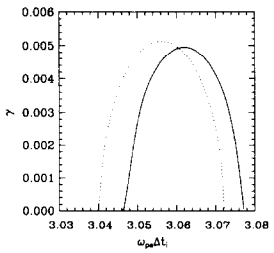

FIG. 2. (b) Growth rate in the vicinity of $\omega_{pe}\Delta t_i = \pi$ for $m_i/m_e = 100$, $k\lambda_D = 0.0982$ and $\Delta t_i/\Delta t_e = 7$. The approximate analytical solution (···) and the numerical solution (—).

Both the approximate analytical solution and the numerical solution are plotted on the same graph. It is clear that the agreement is very good in the cold plasma case. The real part of the frequency is close to ω_{pe} as predicted by the theory. The dependence of the growth rate on the mass ratio is also shown in Fig. 2a. It is easily verified that the maximum growth rate and the domain of instability obey the scaling given by the theory.

In Fig. 3, the growth rate is shown as a function of $\omega_{pe}\Delta t_i$ for two different values of the electron time step. Here again, the agreement with the theory is very good.

We also checked the dependence of the value of $\omega_{pe}\Delta t_i$ corresponding to the maximum growth rate as well as the value of this growth rate as a function of $k\lambda_D$ for two values of the mass ratio. This is illustrated in Figs. 4 and 5; the agreement with the approximate solution is good except when $k\lambda_D$ becomes larger than 0.2, in which case Landau damping begins to play a role and finally suppresses the instability.

4.3 *Study of Dispersion Relation around* 2π

In this case it is the ion acoustic branch which is destabilized by coupling to two Langmuir waves. We take $\omega \simeq \omega_{pi}$ and $\omega \ll kV_e \ll \Delta t_e^{-1}$, so that $1 + \chi_e^{-1}(\omega) = 1 + k^2\lambda_D^2$ in the $q = 0$ term. For the Langmuir waves ($q = \pm 1$) we assume $\omega_{\pm 1} \gg kV_e$ (i.e., $kV_e\Delta t_i \ll 1$), so that

$$\chi_e^{-1}(\omega_{\pm 1}) \simeq A \mp 2\omega/\omega_{pe} \qquad \text{with} \qquad A = 1 - ((2/\omega_{pe}\Delta t_e)\sin \pi/N)^2.$$

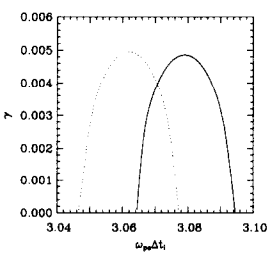

FIG. 3. Growth rate as a function of $\omega_{pe}\Delta t_i$ in the vicinity of π for $m_i/m_e = 100$, $k\lambda_D = 0.0982$, and two different values of $\Delta t_i/\Delta t_e$; $\Delta t_i/\Delta t_e = 7$ (···) and $\Delta t_i/\Delta t_e = 15$ (—).

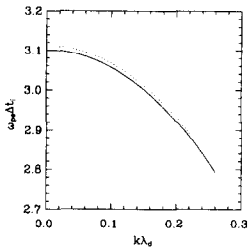

FIG. 4. Value of $\omega_{pe}\Delta t_i$ corresponding to the maximum growth rate in the vicinity of π, as a function of $k\lambda_D$ for two different values of the mass ratio, $m_i/m_e = 400$ (···), and $m_i/m_e = 100$ (—); $\Delta t_i/\Delta t_e = 7$.

Assuming cold ions, $\chi_i^{-1} \simeq -\omega^2/\omega_{pi}^2$. With $H_2 = H_1$, the dispersion relation becomes

$$-\frac{\omega^2}{\omega_{pi}^2} + \frac{k^2\lambda_D^2}{1+k^2\lambda_D^2} = \frac{\omega^2}{\omega_{pe}^2}\frac{2A}{A^2 - 4(\omega^2/\omega_{pe}^2)}. \tag{21}$$

For simplicity, we seek a root with $|\omega^2| > k^2\lambda_D^2\omega_{pi}^2$. We then find a maximum growth rate

$$\mathrm{Im}(\omega/\omega_{pe}) = \tfrac{1}{2}(\omega_{pi}^2/\omega_{pe}^2)$$

(the same as for $\omega_{pe}\Delta t_i \simeq \pi$) occuring when

$$(\omega_{pe}^2 + k^2V_e^2)\frac{\Delta t_i^2}{4\pi^2} = \frac{(N/\pi)\sin \pi/N)^2}{1+\omega_{pi}^2/\omega_{pe}^2},$$

i.e., when the Bohm–Gross frequency is slightly below $2\pi/\Delta t_i$. This estimate of the maximum growth rate is refined by numerical solutions of the dispersion relation discussed below.

Notice that the smallness of the growth rate is due to the presence of the zero of $H_2(\omega)$ at $\pm 2\pi/\Delta t_i$. If instead $H_2(2\pi/\Delta t_i) > 0$, we can expect growth rates as large as

$$\mathrm{Im}\ \omega \simeq \omega_{pi}(H_2)^{1/2}.$$

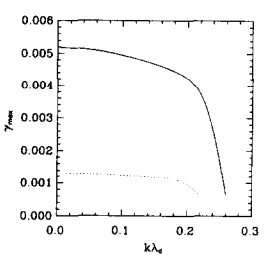

FIG. 5. Maximum growth rate in the vicinity of π as a function of $k\lambda_D$ for two different values of the mass ratio, $m_i/m_e = 400$ (···), and $m_i/m_e = 100$ (—); $\Delta t_i/\Delta t_e = 7$.

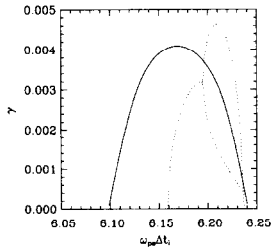

FIG. 6. Growth rate of the numerical instability for $\omega_{pe}\Delta t_i$ in the vicinity of 2π for $k\lambda_D = 0.015$, $\Delta t_i/\Delta t_e = 15$, and $m_i/m_e = 100$. The numerical solution of the full dispersion relation (—), and the approximate analytical solution (···).

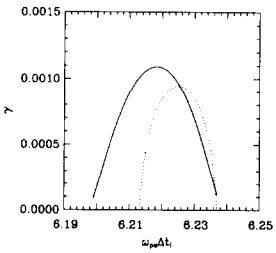

FIG. 7. Same as Fig. 6, but for a mass ratio $m_i/m_e = 400$.

This point has been verified in some simulations by changing the values of the weights in the calculation of the electric field seen by the ions.

In Figs. 6 and 7, we compare the solution of the approximate dispersion relation (21) and the exact (10), (11) dispersion relation. The mass ratio is 100 in Fig. 6 and 400 in Fig. 7. The analytical approximation is much less accurate than for the preceeding case, especially for $m_i/m_e = 100$, where it gives two branches instead of one.

5. COMPARISON OF ANALYSIS AND CODE RESULTS

In order to check the preceeding analysis, we modified a standard PIC code to implement the algorithm considered. The grid size is $\Delta x = \lambda_D$, and the number of cells is 64 so that the longest wavelength that fits into the system is $k\lambda_D = 0.0982$. Most of the study was made with 8192 electrons and ions. The mass ratio m_i/m_e was taken to be either 100 or 400 and the electron time step to be either $\simeq 0.2\omega_{pe}^{-1}$ or $\simeq 0.4\omega_{pe}^{-1}$. Because it is the most straightforward scheme, we only used the odd N algorithm. The results of the simulations agree with the broad features of the theory, such as the domain of instability, the value of maximum growth rate, and its dependence on the mass ratio, but some unexpected modes appear.

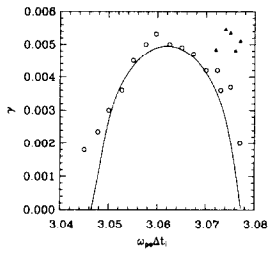

FIG. 8. Comparison of the theory and results of particle simulation in the vicinity of π. The mass ratio is 100, $\Delta t_i/\Delta t_e = 7$, $k\lambda_D = 0.0982$. The data points of the simulation have been separated into two classes: data which fit the theory (○), and points (▲) which seem to indicate the existence of another branch not predicted by the theory.

5.1 *Simulation around* $\omega_{pe}\Delta t_i = \pi$

In Fig. 8, we show data points obtained with $\Delta t_e \simeq 0.44$, i.e., with seven electron time steps during one ion time step, and $a_n \simeq 1/7$. The solid line corresponds to the numerical solution of the warm plasma dispersion relation for $k\lambda_D = 0.0982$, while the dots correspond to simulation data. We notice that the agreement with the theory is good in term of maximum growth rate and of dependence of γ with Δt_i, but we found another branch, with similar growth displayed as triangles on the plot, that is not predicted by the theory.

Similar data obtained with $\Delta t_e \simeq 0.2$, which corresponds to 15 electron time steps during one ion time step, are shown in Fig. 9. The simulation data show that in this case there also seems to exist at least one other unstable branch not predicted by the theory, having a growth rate and domain of instability comparable to the branch predicted by the theory.

We also made a series of runs with a mass ratio of 400 and found that the only unstable mode was the one corresponding to the maximum growth rate predicted by the theory. Outside of the value of $\omega_{pe}\Delta t_i$ corresponding to this growth, no instability was observed. In fact, this is a general result of our simulations; we never observed any instability with a growth rate much smaller than $10^{-3}\omega_{pe}$, close to $\omega_{pe}\Delta t_i = \pi$. This may be an indication that for mass ratio of 900 or over, the instability does not exist, probably due to collisional damping. Finally, let us stress that because of the

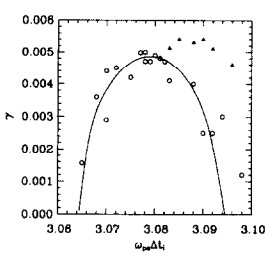

FIG. 9. Same as Fig. 8, but for $\Delta t_i/\Delta t_e = 15$.

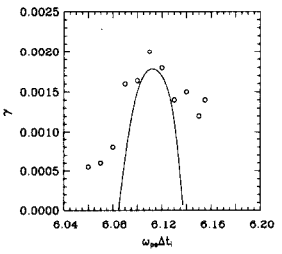

FIG. 10. Comparison of the theory and results of particle simulation in the vicinity of 2π. The mass ratio is 400, $\Delta t_i/\Delta t_e = 15$, $k\lambda_D = 0.0982$. The theoretical result (—), and simulation data points (○).

smallness of the range of instability around π and of the $k\lambda_D$ dependence of the value of $\omega_{pe}\Delta t_i$ corresponding to the maximum growth rate, we never observed the growth of more than one mode at a time.

5.2 *Simulations around* $\omega_{pe}\Delta t_i = 2\pi$

The simulations in the vicinity of $\omega_{pe}\Delta t_i = 2\pi$ were carried out using an electron time step $\Delta t_e \simeq 0.44$, $\Delta t_i = 15\Delta t_e$, $a_n = \frac{1}{15}$, and a mass ratio m_i/m_e of either 100 or 400. In Figs. 10 and 11 is shown a comparison between the curve obtain by solving numerically the dispersion relation (—) and data points obtained from the simulation for $m_i/m_e = 400$ and $m_i/m_e = 100$. The value of the growth rate is in reasonable agreement with the theory. We also measured the value of the real part of the frequency which yielded $\omega \simeq 8 \times 10^{-2}\omega_{pe}$ for $\gamma \simeq \gamma_{max}$ which is not too far from the value 5×10^{-2} obtained from the theory. In fact, the real and imaginary part of the frequency being of the same order of magnitude, their measure is very inaccurate. This is especially true in Fig. 10, where $m_i/m_e = 400$. Similar data are displayed in Fig. 11 for $m_e/m_i = 100$. Agreement with theory is good in the predicted range of instability. Outside of this domain, however, we observed growth which is due to the stronger growth rate of the second spatial Fourier mode; when the fields are filtered to suppress all but mode 1, the *instability* is absent as predicted.

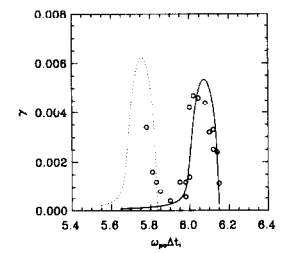

FIG. 11. Same as Fig. 10, but with a mass ratio of 100. The theoretical graph for $k\lambda_D \simeq 0.1$ (—), and for $k\lambda_D \simeq 0.2$ (···); and simulation data corresponding to the mode with $k\lambda_D = 0.1$ (○). Note that below $\omega_{pe}\Delta t_i = 5.85$, the *instability* of mode $k\lambda_D = 0.1$ is driven by the mode $k\lambda_D = 0.2$.

6. Effect of Numerical Damping on the Instability Close to $\omega_{pe}\Delta t_i = \pi$

The instability around $\omega_{pe}\Delta t_i \simeq \pi$ is weak and easily stabilized by collisional damping for large enough mass ratio. It is tempting to see if the introduction of some damping into the electron equation of motion will suppress the instability. Before deciding to do so one has to be aware of the following facts: The limitation $\omega_{pe}\Delta t_i < \pi$ is not serious as long as $m_i/m_e < 400$ because for such values of mass ratio, one is limited by truncation error in $\omega_{pi}\Delta t_i$ more than by stability. For larger mass ratio, there is little to gain in cost of simulation by exceeding the limitation $\omega_{pe}\Delta t_i = \pi$ because once the ions are pushed only once in 10 electron steps, their cost is already negligible.

In [6] it was shown that the following scheme introduces a damping rate $O(\Delta t^3)$:

$$v_{n+1/2} = v_{n-1/2} + a_n \Delta t, \tag{22}$$

$$x_{n+1} = x_n + v_{n+1/2}\Delta t + (\Delta t^2/12)(a_n - a_{n-1}), \tag{23}$$

where a_n is the acceleration computed at time $n\Delta t$. The corresponding damping rate is

$$\mathrm{Im}(\delta\omega/\omega_0) = -\tfrac{1}{24}(\omega_0 \Delta t)^3. \tag{24}$$

It is easy to modify this scheme to introduce a variable damping by using an arbitrary constant in Eq. (23) instead of $\frac{1}{12}$. It becomes [2],

$$x_{n+1} = x_n + v_{n+1/2}\Delta t + c_1 \Delta t^2 (a_n - a_{n-1});$$

the damping rate is then given by

$$\mathrm{Im}(\delta\omega/\omega_0) = -(c_1/2)(\omega_0 \Delta t)^3, \tag{25}$$

while the error on the real part of the frequency remains $O(\Delta t^2)$.

With this numerical damping, the electron susceptibility becomes [6]

$$\chi_e = \chi_0 - \tfrac{1}{12}(\omega_p \Delta t)^2 + c_1 \exp(i\omega\Delta t - \tfrac{1}{2}k^2 V_e^2 \Delta t_e^2). \tag{26}$$

Numerical solutions of the resulting dispersion relation agree with the preceeding estimate (25) for $\omega_{pe}\Delta t_i \simeq \pi$. Close to 2π, the damping is somewhat smaller than this approximate value, probably because it affects the Langmuir waves but not the ion acoustic waves (as can be seen in Eq. (26) with $\omega\Delta t_e \ll 1$).

This scheme is implemented in the electron pusher. In order to distinguish numerical damping from collisional damping, we use the smaller mass ratio $m_i/m_e = 100$ with $\Delta t_e \simeq 0.4$ and $\Delta t_i \simeq \pi$. For $c_1 = 1/24$ and $c_1 = 1/12$, we observed a reduction of the maximum growth rate corresponding to the damping given by (25) and a slight shift of the domain of instability which is reduced simultaneously. Agreement with the theory was found to be good. With a mass ratio of 400 and $c_1 = 1/24$, for which the damping rate is larger than the maximum growth of the

instability, no instability was observed. Similar simulations around 2π demonstrate, in agreement with the theory, that the stabilizing effect of c_1 is somewhat smaller than at $\omega_{pe}\Delta t_i = \pi$ but still exists.

It must also be emphasized that the stabilization is obtained at the expense of a cooling of the electrons. This cooling is related to the value of c_1, and for large values of m_i/m_e, the amount of damping necessary to stabilize the code may be small enough for the cooling to be negligible. Theoretical analysis [2], supports the use of third-order damping as used here to minimize the unwanted cooling, as opposed to simpler, first-order schemes.

7. Future Directions

In order to make further gains in speed, the time spent moving electrons must be reduced. Increasing Δt_e is a limited option, as the explicit electron time integration behaves poorly as Δt_e is increased, even well below the threshold of numerical instability [7]. Implicit schemes seek to remove this limitation, but their application is restricted by the electron transit-time limitation, $kv\Delta t \lesssim 1$ [1, 2]. Perhaps a combination of the two approaches would be fruitful. We propose the following as an example:

A cycle begins with electrons at time $n\Delta t_i - M\Delta t_e$, and ions at $n\Delta t_i$, advanced explicitly using E_{n-1}. A prediction is made for E_n using the principles of an implicit field algorithm [1, 2] with $\rho_{i,n}$ and electron information at time $n\Delta t_i - M\Delta t_e$.

This E_n permits integration of the electrons forward to time $n\Delta t_i + M\Delta t_e$, accumulating along the way a filtered electron charge density to form $\rho_{e,n}$. If this $\rho_{e,n}$ and $\rho_{i,n}$ are sufficiently compatible with the predicted E_n, then E_n is used to advance the ions to time $(n+1)\Delta t_i$ by an explicit scheme to complete the cycle.

What are the advantage relative to the simpler subcycling described in this paper? In addition to the possibility of using fewer electron steps, as noted earlier, the computation cost per time step may be lower. Because the same electric field E_n is used for all the electron steps, one may integrating each electron all N steps at once, rather than having to access the entire electron particle list N times. In large simulations, the particle data commonly reside in disk storage, whose access rates result in considerable overhead on recent computers with very fast central processors. Perhaps the number of electrons needed could be reduced, as was found with *orbit averaged* codes [8], whose implicit version [9] is related to the algorithm proposed here.

References

1. R. J. Mason, *J. Comput. Phys.* **41** (1981), 233; *Phys. Fluids* **23** (1980), 2204; J. Denavit, *J. Comput. Phys.* **42** (1981), 337.

2. A. FRIEDMAN, A. B. LANGDON, AND B. I. COHEN, *Comments Plasma Phys. Controlled Fusion* **6** (1981), 225; B. I. COHEN, A. B. LANGDON, AND A. FRIEDMAN, *J. Comput. Phys.*, in press; A. B. LANGDON, B. I. COHEN, AND A. FRIEDMAN, submitted.
3. A. GOURDIN SERVENIERE AND J. C. ADAM, *Phys. Fluids*, to appear.
4. J. M. DAWSON *et al.*, private communication.
5. A. B. LANGDON, *Phys. Fluids* **22** (1979), 163.
6. A. B. LANGDON, *J. Comput. Phys.* **30** (1979), 202.
7. R. W. Hockney and J. W. Eastwood, "Computer simulation using particles," McGraw–Hill, New York, 1981.
8. B. I. COHEN, T. A. BRENGLE, D. B. CONLEY, AND R. P. FREIS, *J. Comput. Phys.* **38** (1980), 45.
9. B. I. COHEN, R. P. FREIS, AND V. THOMAS, UCRL 86429 (1981); *J. Comput. Phys.*, to appear.